DOI 10.1007/s10511-016-9441-x
Astrophysics, Vol. 59, No. 3, September, 2016

THE OBJECT CLN 138 – A DOUBLE STAR-FORMATION REGION

A. L. Gyulbudaghian

A double star formation region associated with the biconical cometary nebula CLN 138 is studied. ^{12}CO(1-0) observations of a molecular cloud associated with this object reveal the existence of several molecular clouds in this region, as well as the existence of red and blue molecular outflows. Several new Herbig-Haro objects are found, two of which have undergone a luminosity increase of at least 8^m. The first star formation region is basically embedded in the molecular cloud; most of the stars in it are infrared stars and many have dust envelopes. The second star formation region has already left the molecular cloud; it has no IR stars and few of its stars have dust clouds.

Keywords: *star formation region: molecular outflow: Herbig-Haro objects*

1. Introduction

There are two kinds of star formation regions [1]: (1) regions in which stars with high masses are formed (these are encountered in giant molecular clouds, GMC) and (2) regions in which stars with intermediate and low masses are formed (these are mainly encountered in molecular clouds and dark globules). A double star formation region of the second kind associated with the cometary nebula CLN 138 [2,3] (see Figs. 1 and 2) is examined in this article. A molecular cloud associated with CLN 138 is also studied.

V. A. Ambartsumyan Byurakan Astrophysical Observatory, Armenia; e-mail: agyulb@bao.sci.am

Original article submitted April 27, 2016; accepted for publication June 22, 2016. Translated from Astrofizika, Vol. 59, No. 3, pp. 403-412 (August 2016).

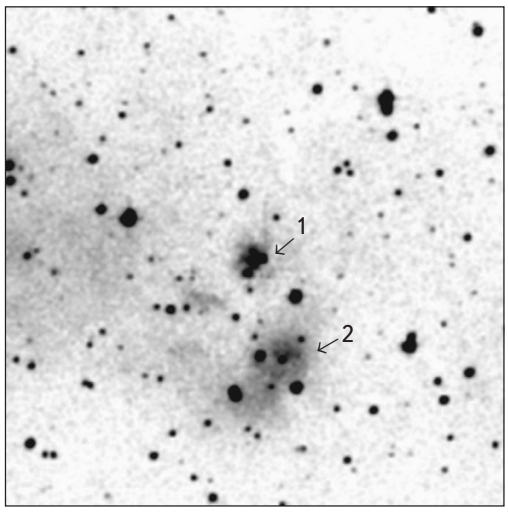

Fig. 1. A DSS2 R image of the region containing the object CLN 138: (1) first star formation region, (2) second star formation region. North is upward, east to the left. The image size is 6'×6'.

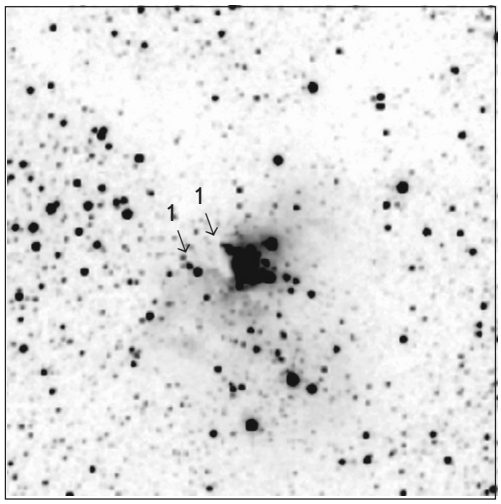

Fig. 2. A 2MASS K image of the region containing the object CLN 138: the biconical cometary nebula is indicated by the labels "1." North is upward, east to the left. The image size is 6'×6'.

2. ^{12}CO(1-0) observations of the molecular cloud associated with the object CLN 138

^{12}CO(1-0) observations in Chile of southern objects have been quite productive: molecular outflows have been discovered, as well as rotation of molecular clouds [4,5]. ^{12}CO(1-0) observations of the molecular cloud associated

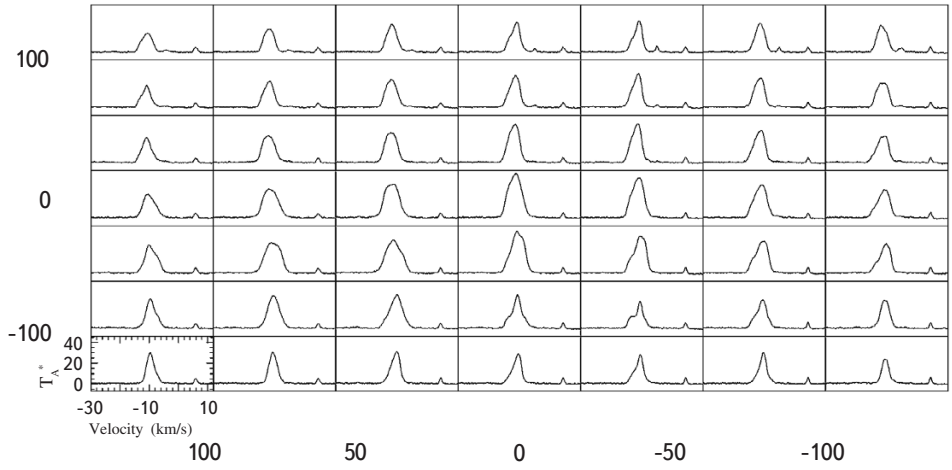

Fig. 3. ^{12}CO(1-0) spectra of part of the molecular cloud surrounding CLN 138.

with the object CLN 138 were made on August 30, 2003, at the 15-m SEST (Sweden-ESO submillimeter telescope) telescope in Cerro la Silla, Chile. The directional diagram of the antenna at 115 GHz is ~45° and the beam efficiency is 0.70. The position and direction of the source were observed with a step size of 40" in a frequency modulation regime with a frequency spread of 10 MHz. During the observations the telescope was equipped with an SIS detector and a high-resolution acousto-optical spectrometer (with 1000 channels and a velocity resolution of 0.112 km/s). These observations were made with Prof. Jorge May (National Observatory of Chile, Santiago, Chile).

Figure 3 shows spectra derived from ^{12}CO(1-0) observations of the molecular cloud associated with CLN 138. Figure 3 can be used to find the velocity distribution in this region. The cells in Table 1, which list the radial velocities in km/s, correspond to the cells of Fig. 3. It can be seen from Fig. 3 that there are three peaks (i.e., three clouds): one with a velocity of about -10.32 km/s (the main cloud), a second with a velocity of about -4.10 km/s, and a third with a velocity of about 5.95 km/s. The cloud with a velocity of 5.95 km/s is distributed uniformly over the entire region of study with roughly the same velocity and the same antenna temperature (4 K), so we do not include it in Table 1. This table includes data on the two other clouds with average velocities of -10.32 and -4.10

TABLE 1. Distributions of ^{12}CO(1-0) Velocities in the Molecular Cloud Surrounding CLN 138

-10.74 -4.32	-11.17 -3.89	-10.74 -4.32	-9.89 -3.89	-10.32 -3.89	-10.74 -4.32	-10.74 -4.32
-11.17 -3.89	-11.17	-10.74	-10.32 -3.89	-10.32 -3.89	-10.74 -4.32	-10.74 -4.32
-11.17	-11.6	-11.17	-10.74	-10.74 -3.89	-10.74	-9.89
-10.74	-11.17	-10.74	-10.32	-10.32	-10.32	-9.46
-9.89	-11.17	-10.32	-9.89	-9.46	-9.46	-9.03
-9.46	-9.89	-9.03	-9.89	-9.89	-9.89	-9.46
-9.89	-9.89	-9.46	-9.46	-9.89	-9.46	-9.46

TABLE 2. Distribution of the Antenna Temperature in the Molecular Cloud Surrounding CLN 138

18.18	3.64	23.04	1.21	25.35	4.85	26.56	3.64	30.20	4.85	27.77	3.64	26.56	6.06
20.61	2.42	25.35		26.56		30.20	3.64	31.41	3.64	37.78	3.64	24.24	2.42
23.04		25.35		28.99		36.36		36.36	2.42	30.20		25.35	1.21
23.04		27.78		31.41		42.42		40.00		32.62		26.56	
26.56		28.99		31.41		40.00		33.84		30.20		27.78	
27.78		30.20		32.62		33.84		25.35		27.78		26.56	
30.20		30.20		31.41		27.78		27.78		30.20		23.04	

km/s, respectively.

Table 1 shows that the main cloud is distributed over the entire region, but the cloud with an average velocity of -4.10 km/s appears only in the northern part of the observed region, along an E-W direction. In order to give a better idea of the distribution of the clouds in this region, Table 2 lists the antenna temperatures of the radiation from these clouds. The cells in Table 2 are the same as in Table 1. The antenna temperatures are given in units of 1.21 K.

Table 2 shows that the maximum antenna temperature in the main cloud belongs to the object CLN 138 and that the antenna temperature falls off toward the periphery of the cloud.

Table 3 shows that, besides the main emission at approximately -10.32 km/s, in the main cloud there is also a red outflow with velocities in the interval -15.05 to -12.03 km/s, or -4.72 to -1.71 km/s relative to the velocity of the main cloud and a blue outflow with velocities in the interval -9.03 to -6.02 km/s, or 1.02 to 4.30 km/s relative to the velocity of the main cloud. Table 3 lists the antenna temperatures for the red and blue outflows. The cells in Table 3 are the same as in Table 1, with the blue outflow data on the left and the red outflow data on the right. Table 3 shows that the red shift is smaller than the blue outflow in terms of the area it occupies and is less intense

TABLE 3. Distribution of the Antenna Temperature Along the Red and Blue Molecular Outflows

				2.42		3.64							2.42
		2.42				2.42		2.42		3.64			
	2.42	2.42		1.21		2.42		2.42		6.06			
2.42	2.42	6.06		2.42		3.64		3.64		7.27			
3.64	3.64	2.42	2.42	1.21	2.42	4.85		4.85		7.27			
2.42				3.64	2.42	6.06		4.85					
				1.21		3.64							

than the blue outflow (the maximum antenna temperature for the red outflow is 3.64 K and for the blue outflow, 7.27 K). This can be explained by the fact that the red outflow from the source is directed into the molecular cloud, where the absorption is greater, while the blue outflow is directed toward us, i.e., the absorption should be smaller for it.

3. The object CLN 138 and the two star formation regions associated with it

This object lies in a molecular cloud which is part of the Sco OB4 association [3]. The OB-association Sco OB4 is at a distance of 1180 pc [6], so that CLN 138 is at approximately the same distance. In Figs. 1 and 2 there are two star formation regions in this region. CLN 138 itself is mostly in a dark cloud. In Fig. 2, this object appears as a biconical cometary nebula with its northern half less immersed in the cloud than the southern half, since it can be seen in the 2MASS K image that the southern half is poorly visible, even in the IR, i.e., it can hardly be seen because of high absorption.

3.1. The region associated with CLN 138. Figures 1 and 2 show that this star formation region is mainly embedded in a dark cloud, with many objects visible only in the IR. It might be expected that young stars surrounded by dust disks/envelopes might be found in this region.

TABLE 4. Color of Objects from the First Star Fformation Region

N	α(2000)	δ(2000)	*B*	*B* - *V*	*B* - *R*	*J*	*J* - *H*	*H* - *K*	*Q*
1	$17^h17^m00^s.53$	-36°20'44".2				12.355	2.611	1.820	-0.483
2	17 17 01.26	-36 20 51.6	16.39	0.82		13.395	0.492	0.704	-0.705
3	17 17 01.65	-36 20 57.8				12.239	1.756	1.266	-0.396
4	17 17 01.81	-36 20 51.0			*R* = 12.28				
5	17 17 01.92	-36 20 52.1	20.02		8.54	12.577	1.613	1.010	-0.104
6	17 17 02.01	-36 21 04.0				13.208	1.398	2.084	-2.145
7	17 17 02.07	-36 21 13.5	18.38	1.08	0.81	14.810	2.471	1.795	-0.580
8	17 17 02.14	-36 21 07.5	20.16		1.43	12.662	2.287	1.693	-0.591
9	17 17 02.21	-36 20 51.3			*R* = 13.10				
10	17 17 02.22	-36 20 55.5	18.52		7.03				
11	17 17 02.37	-36 20 53.5			*R* = 13.42				
12	17 17 02.43	-36 21 02.7				12.580	1.789	1.256	-0.346
13	17 17 02.48	-36 20 57.8				14.050	2.787	1.381	0.439
14	17 17 02.64	-36 20 59.0				13.694	2.531	1.356	0.226
15	17 17 02.68	-36 21 15.8	17.55			15.538	1.690	3.047	-3.490
16	17 17 03.01	-36 21 05.5	18.45		7.55				

The free reddening variable $Q=(J-H)-1.7(H-K)$ has been introduced in Ref. 7. If $Q < -0.10$ for a given star, then a dust disk surrounds the star [7]. Table 4 lists the colors of objects in the first star formation region (data from Ref. 8).

The first column of Table 4 gives the sequence number of the objects; the second and third, their coordinates; columns 4-9, their colors; and column 10, the value of Q.

The stars in the first star formation region which are listed in Table 4 include those detectable in the visible and those detectable only in the IR. The following stars are visible in the IR: Nos. 1, 3, 6, 12, 13, and 14. The following stars have a dust disk (as stated above, it is necessary that $Q < -0.10$ for a star to have a dust disk): Nos. 1, 2, 3, 5, 6, 7, 8, 12, 13, and 15; that is, all the stars that are detectable in the visible and all the IR stars, except No. 14, have dust disks. The central star in the biconical nebula is star No. 15. According to Table 4, this star has the highest value of $H-K$, which may indicate that the star lies behind a dense dust disk; this is also indicated by its having the lowest value of Q.

3.2. The second star formation region. In Figs. 1 and 2 this region is mainly outside the dark cloud. Table 5 lists the colors of objects in the second star formation region (data from Ref. 8). The first column of the table gives the sequence number of the objects; the second and third, their coordinates; columns 4-9, their colors; and column 10, the value of the above-mentioned parameter Q.

There are no IR stars among the stars in the second star formation region. Stars 2 and 6 have dust disks, but stars 1, 3, 7, and 9 do not have disks. Thus, in the first region only one of 11 stars does not have a dust disk, but of the 6 stars in the second region, 4 do not have dust disks.

TABLE 5. Color of Objects from the Second Star Formation Region

N	α(2000)	δ(2000)	*B*	*B - V*	*B - R*	*J*	*J - H*	*H - K*	*Q*
1	$17^h16^m59^s.06$	-36°21'49".6	17.40	0.75	3.55	14.608	0.602	0.323	0.053
2	17 16 59.26	-36 22 23.9	16.37	1.51	1.79	9.101	0.983	0.713	-0.229
3	17 17 00.17	-36 22 03.0	16.93	-0.04	2.19	12.762	0.945	0.560	-0.007
4	17 17 00.64	-36 21 59.8	16.92		7.38				
5	17 17 00.83	-36 22 23.7	19.10		2.97				
6	17 17 01.47	-36 22 01.4	16.58	0.73	2.32	11.563	0.630	0.457	-0.147
7	17 17 01.75	-36 22 56.8	18.11	0.83		11.436	2.574	1.335	0.304
8	17 17 02.90	-36 22 30.0	14.43		0.07				
9	17 17 03.1	-36 22 27.0	14.48	0.77	-0.07	12.672	0.535	0.182	0.236

3.3. Relationship to the IRAS source. CLN 138 is associated with the source IRAS 17136-3617 [9]. A method has been proposed [10] for classifying IR sources based on their IR colors. Three quantities were introduced: $R(1,2) = \log((F(25)\times 12)/(F(12)\times 25))$, $R(2,3) = \log((F(60)\times 25)/((F(25)\times 60))$, and $R(3,4) = \log((F(100)\times 60)/(F(60)\times 100))$. These parameters lie within definite ranges for different types of IR sources: (1) objects associated with water masers have $R(1,2) = (0.2 - 0.8)$, $R(2,3) = (0 - 1.3)$, and $R(3,4) = (-0.3 - 0.3)$; (2) T Tauri-type stars have $R(1,2) = (-0.25 - 0.15)$, $R(2,3) = (-0.5 - 0.1)$, and $R(3,4) = (-0.25 - 0.2)$; (3) cold unevolved sources in dark clouds have $R(3,4) > 0.3$. For IRAS 17136-3617 we have $R(1,2) = 0.687$, $R(2,3) = 0.260$, and $R(3,4) = -0.125$. These values lie within the intervals corresponding [10] to the first type of objects, i.e., objects associated with water masers.

3.4. Herbig-Haro (H-H) objects in both star formation regions. In the spectra of H-H objects [11] the continuum is either absent or very weak, and strong emission lines are present: $H\alpha(6563A)$, [NII] (6548, 6584), [SII] (6717, 6731), [OI] (6300, 6363), and [OII] (3726, 3729). The Hα, [NII], [OI], and [SII] lines lie in the *R* color band, and the [OII] lines, in the *B* band, so H-H objects have *R* and *B* colors; other colors are either absent or very weak. Table 6 lists data on known H-H objects. Column 1 gives the sequence number of the objects; column 2, their designations (each object consists of several densifications); columns 3 and 4, their coordinates; and columns

TABLE 6. *B* and *R* Colors for Known Herbig-Haro Objects

N	Object	α(2000)	δ(2000)	*B*	*B* - *R*
1	HH 7-11	$03^h29^m05^s.45$	$31^o15'46".2$	$18^m.81$	$4^m.64$
2	"-"	03 29 06.32	31 15 37.1	19.80	4.48
3	"-"	03 29 08.08	31 15 30.0	17.82	4.66
4	HH1-HH2	05 36 20.32	-06 45 10.0	13.31	1.49
5	"-"	05 36 21.39	-06 45 36.6	17.61	5.51
6	"-"	05 36 25.07	-06 46 56.5	16.85	4.18
7	"-"	05 36 25.54	-06 45 55.0	21.23	2.39
8	"-"	05 36 25.57	-06 47 13.2	11.96	2.72
9	"-"	05 36 26.45	-06 47 26.0	15.49	4.84
10	HH 32	19 20 29.54	11 02 00.0	15.85	2.35
11	GGD 8	05 50 52.73	03 07 43.8	18.79	5.45
12	"-"	05 50 53.95	03 08 00.3	18.86	8.07
13	"-"	05 50 54.19	03 08 04.2	17.36	7.05
14	GGD 12	06 10 50.20	-06 12 01.2	18.43	4.57
15	GGD 37	22 56 01.72	62 01 58.0	20.03	5.46
16	"-"	22 56 02.23	62 01 55.8	19.61	6.43
17	"-"	22 56 07.42	62 02 04.3	16.38	4.95

5 and 6, their colors [8].

This table shows that B-R for the known H-H objects lies within the interval 1.49-8.07.

Although the optical and near IR spectra of H-H objects are qualitatively the same, they do differ quantitatively, beginning with "high excitation" H-H objects (HH I, HH 2H, HH 32), in which the intensity ratio [SII]/Ha lies within a range of 0.16-0.34, and going through "low excitation" H-H objects (HH 7), in which this ratio reaches 2.8 [11]. Compared to the spectrum of HH 7, in the spectrum of HH 2H the [OI] (3717, 3731) line is strong, but the [NII], [SII], [OII], and [OI](6300, 6363) lines are weak. This means that *B-R* for HH 2H must be considerably smaller than for HH 7 (as noted above, HH 7 is a low excitation object). Let us test this proposition. According to Table 6, for HH 2H (object No. 8) *B-R* = 2.72, while for HH 7 (object No. 3) *B-R* = 4.66. For the other objects with high excitation, *B-R* is also comparatively low; for HH 1 (object No. 4 of Table 6) *B-R* = 1.49 and for HH 32 (object No. 10 of Table 6) *B-R* = 2.35. Thus, a low value of *B-R* may indicate a high excitation object, and a higher value of *B-R*, a low excitation object.

It can be seen from Tables 4 and 5 that among the objects in the first and second star formation regions some only have colors *B* and *R*. It may be assumed that these are Herbig-Haro objects, since, as noted above, the known H-H objects also have only these colors. For the known H-H objects (Table 6), *B-R* lies within the interval 1.49-8.07, while for the objects in Tables 4 and 5, *B-R* = 0.07-8.54. In Table 4, objects 5, 10, and 16 have low excitation and there are no high excitation objects. Regarding object No. 5 of Table 4, it can be said that here there may be simultaneous detection of emission from two very nearby objects— an H-H object (color *R* and, partially, *B*) and stars (colors *J, H, K*, and, partially, *B*). It is possible that the H-H object has been ejected from this star. In Table 5, No. 4 has low excitation and objects 5 and 8 have high excitation. Among the H-H objects in Tables 4 and 5, some are quite bright in *R* [8], but can barely be seen in the DSS2 R images; these are No. 16 of Table 4 and No. 4 of Table 5. The faintest object in *R* for which data are given in Ref. 8 is object No. 18 of Table 4, for which *R* = 18.33. The two objects named in Fig. 1 are fainter than this object. Given that these objects have *R* magnitudes of about 10^m [8], it appears that their luminosity has increased by more than 8^m. This seems to be an indication of the birth of new H-H objects.

4. Conclusion

This was a study of the double star formation region associated with the biconical cometary nebula CLN 138. Data from $^{12}CO(1-0)$ observations of the molecular cloud associated with this object have been presented. These observations show that two other clouds exist in this region besides the main cloud with its velocity of -10.32 km/s: one with a velocity of -4.10 km/s and the other with a velocity of 5.95 km/s. A red molecular outflow with a velocity of -4.72 to -1.71 km/s relative to the velocity of the main cloud and a blue outflow with a velocity of 1.02 to 4.30 km/s relative to the velocity of the main cloud have been discovered. Several H-H objects have been found in the two regions, including two objects which have undergone a rise in brightness by 8^m, which indicates that we may be dealing with the birth of new H-H objects. In the first region there are 6 IR stars and in the second

there are no IR stars. This suggests that the first region is substantially embedded in the dark cloud, while the second region has mostly emerged from the dark cloud. In an evolutionary sense, the objects in the first region are in an earlier stage of evolution than those in the second region, since the objects in the first region include many more stars with dust envelopes.

REFERENCES

1. N. D. Evans, Protostars and Planets [Russian translation], Mir, Moscow (1982), p. 171.
2. A. L. Gyulbudaghian and T. Yu. Magakian, Pis'ma v Astron. zh. **3**, 113 (1977).
3. A. L. Gyulbudaghian, R. Shvarts, and F. Nazaretyan, Soobshch. Byurakanskoi obs. **63**, 3 (1990).
4. A. L. Gyulbudaghian and J. May, Astrophysics **47**, 352 (2004).
5. A. L. Gyulbudaghian and J. May, Astrophysics **48**, 79 (2005).
6. J. Ruprecht, B. Balazs, and R. E. White, Catalogue of Star Clusters and Associations, Supplement I, Budapest (1970).
7. F. Comeron, N. Schneider, and D. Russel, Astron. Astrophys. **433**, 955 (2005).
8. N. Zacharias, D. G. Monet, et al., The Naval Observatory Merged Astrometric Dataset (2005).
9. IRAS Point Source Catalog, Version 2 (1988), Washington, D.C.
10. J. Wouterloot and C. Walmsley, Astron. Astrophys. **168**, 237 (1986).
11. K.-H. Bohm, Rev. Mex. Astron. Astrofis. **7**, 55 (1983).